MODELING STUDY OF SOLID OXIDE FUEL CELL OPERATING ON REFORMED DIESEL FUEL

Asst. Prof. Cüneyt EZGİ, Nav. Cdr.[1*]
Asst. Prof. M.Turhan ÇOBAN[2]

[*1]*Mechanical Engineering Department, Turkish Naval Academy*
Tuzla, Istanbul, Turkey
[2]*Mechanical Engineering Department, Ege University,*
Bornova, Izmir, Turkey

cezgi@dho.edu.tr, turhan.coban@ege.edu.tr

Abstract

Fuel cells provide great potential for electric power generation on-board ships. Ships use marine diesel fuel for marine main and auxiliary engines . In this work, this paper presents the performance analysis of a planar solid-oxide fuel cell (SOFC) under reformed diesel fuel. A detailed solid-oxide fuel cell model is used to study the influences of various operating parameters on cell performance. Significant differences in efficiency and power density are observed for isothermal operational regimes. In the model, electrochemical kinetics, gas dynamics and species are coupled. The model predicts polarization curve, velocity and species concentration and current distribution in the cell depending on fuel cell temperature and electrodes/ electrolyte materials used in the components

Cüneyt EZGİ, M.Turhan ÇOBAN

YAKIT DÖNÜŞTÜRÜCÜDE DÖNÜŞTÜRÜLMÜŞ DİZEL YAKIT İLE ÇALIŞAN KATI OKSİTLİ YAKIT PİLİNİN MODELLEME ÇALIŞMASI

Özetçe

Yakıt pilleri, gemilerde elektrik gücü üretimi için büyük bir potansiyel sağlamaktadır. Gemiler, ana ve yardımcı makinaları için deniz tipi dizel yakıt kullanmaktadır. Bu çalışmada, yakıt dönüştürücüde dönüştürülmüş dizel yakıtı ile çalışan düzlemsel tip katı oksitli yakıt pilinin performans analizi sunulnuştur. Detaylı bir katı oksitli yakıt pili modeli, çeşitli işletme parametrelerinin hücre performansı üzerindeki etkilerini çalışmak için kullanılmıştır. İzotermal çalışma rejimleri için verim ve güç yoğunluğunda önemli farklar gözlemlenmiştir. Modelde elektrokimyasal kinetikler, gaz dinamiği ve maddeler birleştirilmiştir. Model, yakıt pili sıcaklığına ve bileşenlerde kullanılan elektrod/elektrolit malzemelerine bağlı olarak polarizasyon eğrisini, hızı, madde konsantrasyonlarını ve akım dağılımını tahmin etmektedir.

Keywords: Solid oxide fuel cell, Fuel cell modeling, Diesel fuel

1. Introduction

Fuel cells are electrochemical devices that convert the chemical energy stored in a fuel directly into electrical power. Solid oxide fuel cell (SOFC) is considered as one of the most promising energy conversion device and as an alternative of existing power generation systems. SOFCs operate at high temperatures from 600 to 1000 ^{o}C to ensure sufficient ion conductivity through their electrolytes which are nonconductive to electrons.

Main SOFC components include air channel, cathode, electrolyte, anode, fuel channel, and interconnects. The most common materials used for the SOFC cell components are oxide ion conducting yttria stabilized zirconia (YSZ) for the electrolyte, strontium-doped lanthanum manganite (LSM) for the cathode, and nickel/YSZ for the anode.

During fuel cell operation, oxidant gas (oxygen or air) at the cathode side receives electrons to form oxygen ions that migrate through the electrolyte to the electrolyte/anode interface. Fuel gas (H_2-rich gas) simultaneously fed at the anode side reacts with the oxygen ions to generate steam and electrons. The electron flow in the external circuit from the anode to the cathode produces direct-current electricity.

In general, a SOFC can have either a planar or tubular configuration. The planar design has recently received much attention since it is simpler to fabricate and more flexible in terms of cell geometry. This decreases the ohmic resistance and makes the design better suited for operation at lower temperatures (873–1073 K); the system is referred to as an 'intermediate-temperature solid oxide fuel cell' (IT-SOFC).

SOFCs can be operated on many different fuels. This model describes a unit running on reformed marine diesel fuel.

Nowadays, three basic designs are studied; they are cathode-, electrolyte- and anode-supported designs. The latter design has been considered to be better than any other designs because it can operate at lower temperature and the highest performance can be achieved [2].

SOFC system involves multiphysics phenomena, including the mass balance of diffusion and adsorption of the gases; the electronic/ionic current balance of the interconnects/ current collectors, the electrodes and the electrolyte; the heat transfer and energy balance; and the electrochemical charge transfer reactions.

This model studies the current density distribution in a solid oxide fuel cell (SOFC). It includes the full coupling between the mass balances at the anode and cathode, the momentum balances in the gas channels, the gas flow in the porous electrodes, the balance of the ionic current carried by the oxide ion, and an electronic current balance.

2. Electrochemical Reactions

It is useful to recall the electrochemical processes taking place in the solid oxide fuel cell as illustrated in Figure-1 to begin building an electrochemical model [3]. As shown, fuel and air are admitted to the cell separately. Due to the chemical affinity hydrogen and oxygen have for one another, they are drawn towards the electrodes, diffuse through the porous electrode structure to the electrode/ electrolyte interface and are adsorbed. At the cathode/electrolyte interface, the oxygen is reduced by incoming electrons to produce oxygen anions which are conducted through the solid electrolyte to the anode/electrolyte interface where they electrochemically combine with adsorbed hydrogen to form water vapor and release the electron charge to the external circuit. Because the potential of the electrons released at the anode is greater than that of the electrons taken up by the oxygen at the cathode, the cell delivers net power as electricity.
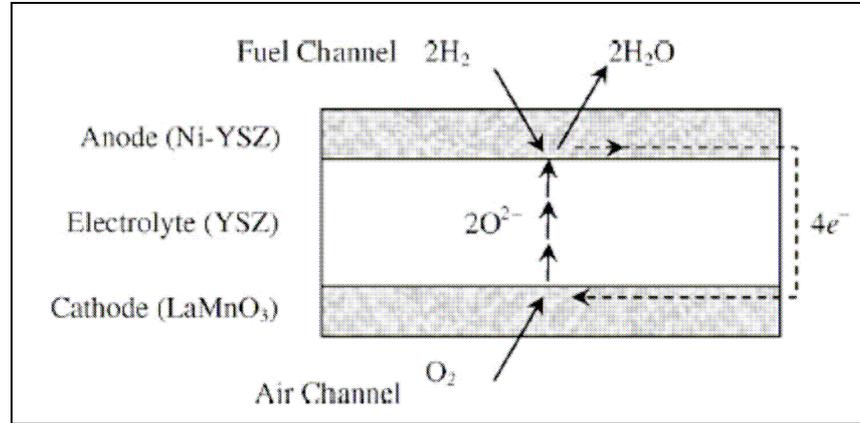
Fig.1.Schematic of electrochemical reactions

At the triple phase boundary (TPB) of cathode/electrolyte/air, if that is where the incorporation of oxygen into the electrolyte occurs,

$$\frac{1}{2}O_2 + 2e^= \rightarrow O^= \tag{1}$$

$$CO + O^= \rightarrow CO_2 + 2e^- \tag{2}$$

Although direct oxidation of CO and hydrocarbons on Ni-based anodes have been demonstrated, these reactions are much slower than hydrogen oxidation, thus it is usually assumed that they do not react directly on the TPB, but they contribute to the overall reaction by producing H_2. However, this reaction is neglected as carbon monoxide oxidation on SOFC anodes has been shown to be 2-5 times slower than that of hydrogen, making the competing and faster water gas shift reaction the dominant reaction pathway for the consumption of carbon monoxide. Therefore, in the present paper, no direct CO and hydrocarbon oxidation is assumed. However, it should be stressed that a recent study of Andreassi et al. demonstrated that, under certain operating conditions, ignoring direct oxidation of CO can lead to a significant underestimation of the voltage [4].

61

After oxygen ions transfer from the cathode side to the anode side through the electrolyte, the following reaction occurs at the TPB of anode/electrolyte/fuel:

$$H_2 + O^= \rightarrow H_2O + 2e^- \tag{3}$$

$$H_2 + \frac{1}{2}O_2 \rightarrow H_2O \tag{4}$$

3. Mathematical model

An SOFC is constructed with two porous electrodes with an electrolyte in the middle. The fuel feed in the cathode and anode is counter-flow, with hydrogen-rich anode gas entering from the left. The model includes the following processes:

- •Electronic charge balance
- •Ionic charge balance
- •Butler-Volmer charge transfer kinetics
- •Flow distribution in gas channels
- •Flow in the porous electrodes
- •Mass balances in gas phase in both gas channels and porous electrodes

3.1 Charge Balances

The electronic charge balance in the anode and cathode current feeders is given by

$$\nabla.\left(-\kappa_1 \nabla \Phi_{electronic}\right) = 0 \tag{5}$$

where κ_1 denotes the electronic conductivity of the current feeder and is its electronic potential.

Similarly, the ionic charge balance, valid in the ionic conductor is

$$\nabla.\left(-\kappa_2\nabla\Phi_{ionic}\right)=0 \tag{6}$$

where κ_2 is the ionic conductivity and is the ionic potential.

In the anode and cathode electrodes, electrons are transferred between the ionic conducting electrolyte phase and the electronically conducting phase. This implies that the charge balance equations have current source terms present as:

$$\nabla.\left(-\kappa_1\nabla\Phi_{electronic}\right)=S_a.i_{ict} \tag{7}$$

$$\nabla.\left(-\kappa_2\nabla\Phi_{ionic}\right)=S_a.i_{ict} \tag{8}$$

where $S_a.i_{ict}$ denotes the specific surface area S_a times the charge transfer current reaction density, i_{ict}.

Butler-Volmer charge transfer kinetics describe the charge transfer current density. At the anode, hydrogen is reduced to form water, and the following charge transfer kinetics equation thus applies:

$$i_{a,ct}=i_{o,a}.x_{h2}\frac{c_t}{c_{h2,ref}}\left[\exp\left(\frac{0,5F}{RT}\eta\right)-\exp\left(\frac{-0,5F}{RT}\eta\right)\right] \tag{9}$$

$$i_{c,ct}=i_{o,c}.\left[\exp\left(\frac{0,5F}{RT}\eta\right)-x_{o2}\frac{c_t}{c_{o2,ref}}\exp\left(\frac{-0,5F}{RT}\eta\right)\right] \tag{10}$$

where $i_{0,c}$ is the cathode exchange current density (A/m^2), and x_{o2} is the molar fraction of oxygen. The overvoltage is defined as

$$\eta = \Phi_{electronic} - \Phi_{ionic} - \Delta\Phi_{eq} \tag{11}$$

$$\eta_a = \Phi_{electronic} - \Phi_{ionic} - \Delta\Phi_{eq-a} \tag{12}$$

$$\eta_c = \Phi_{electronic} - \Phi_{ionic} - \Delta\Phi_{eq-c} \tag{13}$$

$$V_{cell} = \Delta\Phi_{eq,c} - \Delta\Phi_{eq,a} - V_{pol} \tag{14}$$

where V_{pol} is the polarization.

3.2 Multicomponent Transport

This model describes a unit running on hydrogen rich gas reformed diesel fuel and air. At the anode, the gas consists of five components: hydrogen, water vapor, carbon monoxide, carbon dioxide and nitrogen. In the cathode, the gas consists of two components: oxygen and nitrogen.

Fick's law is based upon the assumption that species dissolved in a solution or gas stream interact only with the solvent or the carrier gas. The diffusion coefficients describing such interactions are independent of concentration. Yet, in concentrated solutions or gas mixtures, where relative concentrations are of the same order of magnitude, all species interact with each other and themselves. Their diffusion coefficients are therefore species and concentration dependent, and can also depend on temperature and pressure.

Mass transport equation:

$$\frac{\partial}{\partial t}(\rho\omega_i) + \nabla.(j_i + \rho\omega_i u) = R_i \tag{15}$$

Above, ji describes the diffusion-driven transport, as outlined by [5]. This transport is a function of temperature and a diffusional driving force dj:

$$j_i = \left(- D_i^T \nabla \ln T\right) - \rho_i \sum_{j=1}^{n} \tilde{D}_{ij} d_j \qquad (16)$$

$$\frac{\partial \rho \omega_i}{\partial t} + \nabla \cdot \left(\rho \omega_i u - \rho \omega_i \sum_{j=1}^{n} \tilde{D}_{ij} \left(\nabla x_j + \left(x_j - \omega_j\right)\frac{\nabla p}{p} \right) - D_i^T \frac{\nabla T}{T} \right) = R_i \quad (17)$$

the species molar fraction, xj, and its gradient can be expressed in terms of the mass fractions ωj:

$$x_j = \frac{\omega_j}{M_j} \cdot M \qquad (18)$$

$$\nabla x_j = \frac{M^2}{M_j} \cdot \sum_{\substack{j=1 \\ k \neq j}}^{n} \left[\frac{1}{M} + \omega_k \left(\frac{1}{M_k} - \frac{1}{M_j} \right) \right] \nabla \omega_k \qquad (19)$$

This all implies that the only dependent variable in the application mode is the mass fraction ω, while the temperature field, T, the pressure field, p, and the velocity, u, are obtained in combination with energy, momentum, and continuity equations.

$$\sum_{i=1}^{n} \omega_i = 1 \qquad (20)$$

The final species is solved through the fact that:

$$\omega_n = 1.0 - \sum_{i=1}^{n-1} \omega_i \qquad (21)$$

65

In the stationary case, the mass balance is governed by:

$$\nabla \cdot \left(w_i \rho u - \rho w_i \sum_{j=1}^{k} \tilde{D}ij \left(\frac{M}{M_j} \left(\nabla w_j + w_j \frac{\nabla M}{M} \right) + \left(x_j - w_j \right) \frac{\nabla p}{p} \right) \right) = R_i \ (22)$$

where represents the ij component of the multicomponent Fick diffusivity, which is calculated from the Maxwell-Stefan diffusivities, Dij (m^2/s), ρ is the density of the fluid (kg/m^3), p the pressure (Pa), and R_i is the reaction source term for species i (kg/m^3·s), and x_j the molar fraction of species j. The average molecular weight is calculated as:

$$M = \sum_{j=1}^{k} x_j M_j \tag{23}$$

As an example, the component in a ternary system is given by:

$$\tilde{D}_{12} = \frac{\dfrac{\omega_1 \left(\omega_2 + \omega_3 \right)}{x_1 D_{23}} + \dfrac{\omega_2 \left(\omega_1 + \omega_3 \right)}{x_2 D_{13}} - \dfrac{\omega_3^2}{x_3 D_{12}}}{\dfrac{x_1}{D_{12} D_{13}} + \dfrac{x_2}{D_{12} D_{23}} + \dfrac{x_3}{D_{23} D_{13}}} \tag{24}$$

The Maxwell-Stefan diffusivities can be described with an empirical equation based on the kinetic gas theory:

$$D_{ij} = k \frac{T^{1.75}}{p \left(v_i^{1/3} + v_j^{1/3} \right)^2} \left[\frac{1}{M_i} + \frac{1}{M_j} \right]^{1/2} \tag{25}$$

where *k* is a constant with the value 3.16·10^{-8} Pa·m^2/s, *T* is the temperature expressed in kelvin, *p* denotes the pressure (Pa), v_i equals the molar

diffusion volume of species i expressed in m^3/mol, and M_i is the molar mass of species i expressed in kg/mol. The molar diffusion volumes are given in Table 1 [6].

Table 1
Diffusion volumes

Species	Diffusion Volume (m^3/mol)
H_2	$6.12.10^{-6}$
N_2	$18.5.10^{-6}$
O_2	$16.3.10^{-6}$
CO	$18.0.10^{-6}$
CO_2	$26.9.10^{-6}$
H_2O	$13.1.10^{-6}$

Assume the gas to be ideal, so that that the density is given by

$$\rho = \frac{p.M}{R.T} \tag{26}$$

In the open channels, set the reaction source term to zero. However, in the electrodes, the source term is given by the electrochemical reaction rate. It is calculated from the charge transfer current density according to Faraday's law

$$R_i = v_i \frac{i_{ct,i} M_i}{n_i F} \tag{27}$$

where v_i is the stoichiometric coefficient and n_i is the number of electrons in the reaction. The boundary conditions at the walls of the gas channel and electrode are zero mass flux (insulating condition). At the inlet, the composition is specified, while the outlet condition is convective flux. This assumption means that the convective term dominates the transport

67

perpendicular to this boundary. Continuity in composition and flux apply for all mass balances at the interfaces between the electrodes and the channels.

3.3 Momentum transport

To model the flow profile in the gas channels and the porous electrodes, The Weakly Compressible Navier-Stokes equation was employed.

$$\frac{\partial \rho}{\partial t} + \nabla.(\rho.u) = 0 \tag{28}$$

$$\rho \frac{\partial u}{\partial t} + \rho u.\nabla u = -\nabla p + \nabla.\left(\eta\left(\nabla u + (\nabla u)^T\right) - \left(\frac{2}{3}\eta - \kappa_{dv}\right)(\nabla.u)I \right) + F \tag{29}$$

The stress tensor used in Equation 27 describes a Newtonian fluid, with an added term κ_{dv}. This term expresses the deviation from Stokes' assumption, which states that the fluid particles are in thermodynamic equilibrium with their neighbors. It is very rare that a fluid shows a significant deviation from Stokes' assumption, and κ_{dv} is therefore by default set to zero.

An important dimensionless number in fluid dynamics is the Mach number, Ma, defined by

$$Ma = \frac{|u|}{a} \tag{30}$$

where a is the speed of sound.

A flow is formally incompressible when Ma = 0. This is theoretically achieved by letting the speed of sound tend to infinity. The Navier-Stokes equations will then have the numerical property that a disturbance anywhere in the computational domain will instantaneously spread to the entire domain. This results in a parabolic equation system.

3.3.1 Gas-flow in the gas channels

The weakly compressible Navier-Stokes equations govern the flow in the open channels:

$$\nabla.(\rho.u) = 0 \tag{31}$$

$$\rho(u.\nabla)u = \nabla.\left[-pI + \eta\left(\left(\nabla u + (\nabla u)^T\right) - \frac{2}{3}(\nabla.u)I\right)\right] \tag{32}$$

3.3.2 Gas-flow in the porous electrodes

The porous nature inhibits the diffusion rate through the media. The inhibition must be related to two factors: Porosity and tortuosity. At zero porosity (i.e., a complete solid), the effective gas-phase diffusivity must be zero. At a porosity of 1 (i.e., an open volume with no solid), the effective diffusivity must equal the bulk value.

$$\varepsilon = \frac{V_a}{V_a + V_k} \tag{33}$$

where V_a is open volume, V_k is solid volume.

Tortuosity is a measure of the effective average path length though the porous media compared to the linear path length across the media in the direction of transport. The more tortuous the path, the longer the effective path length through the media, and the greater reduction in the effective diffusivity, as illustrated in Figure 2 [7]. The effective diffusivity for gas-phase flow in porous media can be written as

$$D_{eff} = D\frac{\varepsilon}{\tau} \tag{34}$$

where D_{eff} is the effective bulk gas-phase diffusivity in the porous media ε is the porosity (void volume fraction), D is the diffusivity in gas, and τ is the tortuosity. Since tortuosity is a difficult parameter to estimate except through direct experiment, a Bruggeman correlation is often used for fuel cell studies. This relationship assumes τ is proportional to $\varepsilon^{-0.5}$, resulting in the simpler expression

$$D_{i,eff} = D_i \varepsilon^{1,5} \tag{35}$$

The permeability of the porous medium (m^2), can be found in [8].

$$K = \frac{\varepsilon^3}{180(1-\varepsilon)^2} . d_p{}^2 \tag{36}$$
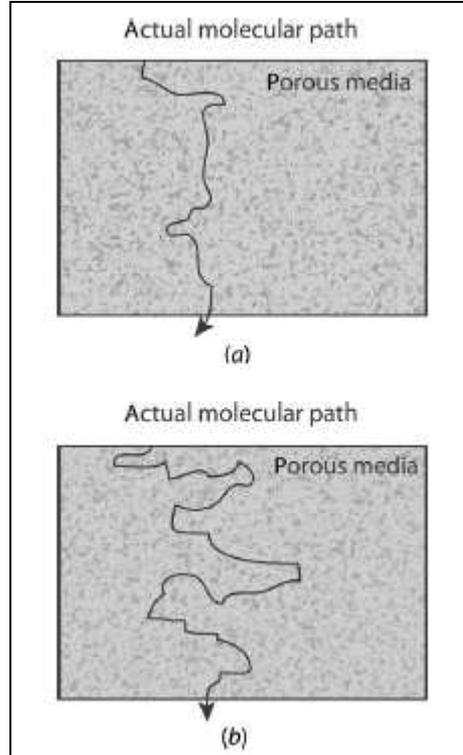
Fig.2. Illustration of porous media with (*a*) low and (*b*) high tortuosity. The Brinkman equations describe flows in porous media, for which the momentum transport within the fluid due to shear stresses is of importance. This mathematical model extends Darcy's law to include a term that accounts for the viscous transport in the momentum balance, and it treats both the pressure and the flow velocity vector as independent variables.

The flow is governed by a combination of the continuity equation and momentum balance equation

$$\frac{\partial}{\partial t}(\varepsilon\rho) + \nabla.(\rho u) = Q \tag{37}$$

$$\nabla.(\rho.u) = Q \tag{38}$$

71

$$\frac{\rho}{\varepsilon}\frac{\partial u}{\partial t}+\left(\frac{\eta}{\kappa}+Q\right)u$$
$$=\nabla\cdot\left[-pI+\frac{1}{\varepsilon}\left\{\eta\left(\nabla u+(\nabla u)^{T}\right)-\left(\frac{2}{3}\eta-\kappa_{dv}\right)(\nabla\cdot u)I\right\}\right]+F \qquad (39)$$

where η and κ_{dv} denote, respectively, the dynamic and dilatational viscosities of the fluid (both in kg/(m·s)), u is the velocity vector (m/s), ρ is the density of the fluid (kg/m^3), p is the pressure (Pa), ε is the porosity, κ is the permeability of the porous medium (m^2), and Q is a mass source or mass sink (kg/(m^3·s)). Influence of gravity and other body forces can be accounted for via the force term F (kg/(m^2·s^2)).

The mass source, Q, accounts for mass deposit and mass creation in subdomains and the mass exchange is assumed to occur at zero velocity.

3.3.3 Model geometry and assumptions

A planar SOFC of counter-flow design was modeled with the dimensions given in Figure 3 and 4. The cell is a typical anode-supported structure with dimensions and materials according to those of an intermediate- temperature SOFC. A 120-kilowatt SOFC system with thermally integrated diesel-fueled reformer and SOFC sub-systems was evaluated. Table 2 lists the results of this evaluation [9].

Table 2
Inlet conditions

Fuel composition [molar fraction]	30 H_2 / 37 H_2O /5 CO / 10 CO_2 / 18 N_2
Air composition [molar fraction]	21 O_2 / 79 N_2
Fuel temperature [°C]	700
Air temperature [°C]	700
Operating pressure [Pa]	1.013×10^5
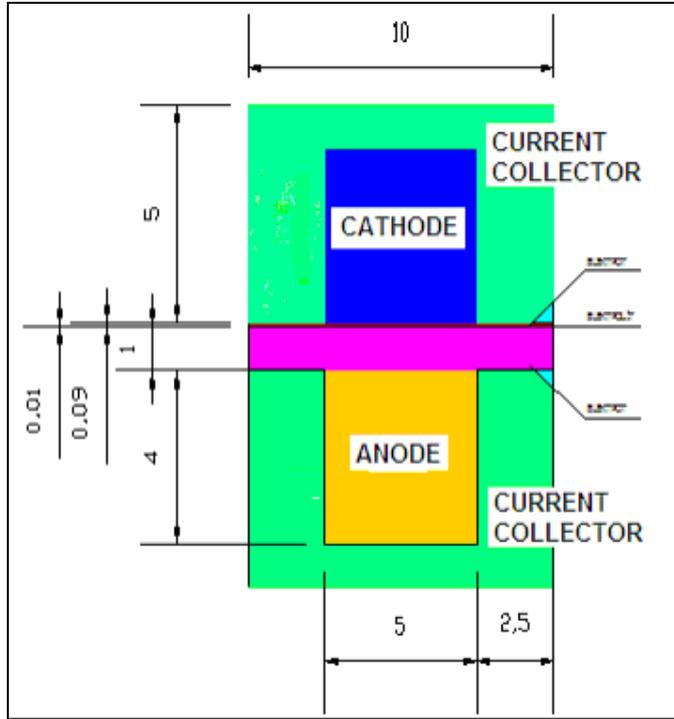
Fig.3. Front view of fuel cell
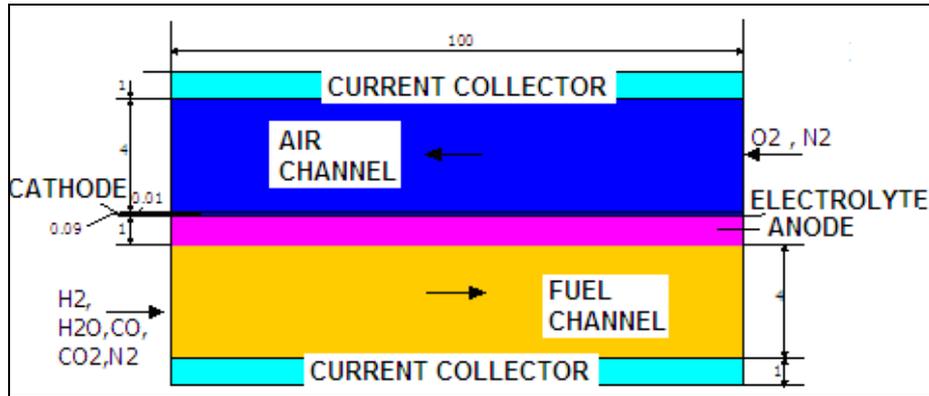
Fig.4. Side view of fuel cell

The specific electric conductivities of cell structure are given in Table 3 together with the assumed materials [10,11,12,13,14].

Table 3
Conductivities and materials assumed for cell components

Cell component	Material	Conductivity
Anode	Ni-YSZ	$\sigma_a = \dfrac{95.10^6}{T} \exp\left(\dfrac{-1150}{T}\right)$
Cathode	LSM (LaSrMnO₃)	$\sigma_c = \dfrac{42.10^6}{T} \exp\left(\dfrac{-1200}{T}\right)$
Electrolyte	8YSZ	$\sigma_e = 3,34.10^4 \exp\left(\dfrac{-10300}{T}\right)$
Current collectors	Stainless steel (X10CrAlSi18)	$\sigma_i = \dfrac{9,3.10^6}{T} \exp\left(\dfrac{-1100}{T}\right)$

The presented model is based on the following assumptions:

- Steady state conditions;
- Pressure drops along the gas channels are 1 Pa at the anode, and 2 Pa at the cathode.
- The cell structure is thin and its temperature is homogeneous in each volume element
- Gas flow is evenly distributed between the channels
- Cell voltage is constant over the bipolar plates.
- All exterior walls are adiabatic.
- No radiated heat between the solid and the gas channels.
- No contact resistance between individual cell components.

Table 4

Model input parameters

Component	Value
k_{katot} (S/m^2)	$2,35.10^{11}$
k_{anot} (S/m^2)	$6,54.10^{11}$
E_{katot} (kJ/mol)	137
E_{anot} (kJ/mol)	140
Anode and Cathode Porosity, ε	0.30
Equilibrium voltage, anode $\Delta\Phi_{eq;a}$, (V)	0
Equilibrium voltage, cathode $\Delta\Phi_{eq;c}$, (V)	0,9
Initial cell polarization, V_{pol}, (V)	0,05
Anode specific surface area, S_{a_a}, (1/m)	1.10^3
Cathode specific surface area, S_{a_c}, (1/m)	$1,1.10^4$
Anode spherical particulate diameter, d_p (m)	$2,5.10^{-6}$
Cathode spherical particulate diameter, d_p (m)	$2,5.10^{-6}$

4. Methods of solution

The governing equations that model a SOFC are highly non-linear and self-coupled, which make it impossible to obtain analytically exact solutions. Therefore, the equations must be solved by discretization thus converting them to a set of numerically solvable algebraic equations. The appropriate solution algorithm to solve a system of partial differential equations strongly depends on the presence of each term and their combinations.

5. Results

Figure 5 and 6 shows the oxygen and nitrogen concentration in the cathode at a cell voltage of 0.5 V, respectively. The oxygen depletion is substantial, which has implications on the reaction distribution at the cathode.
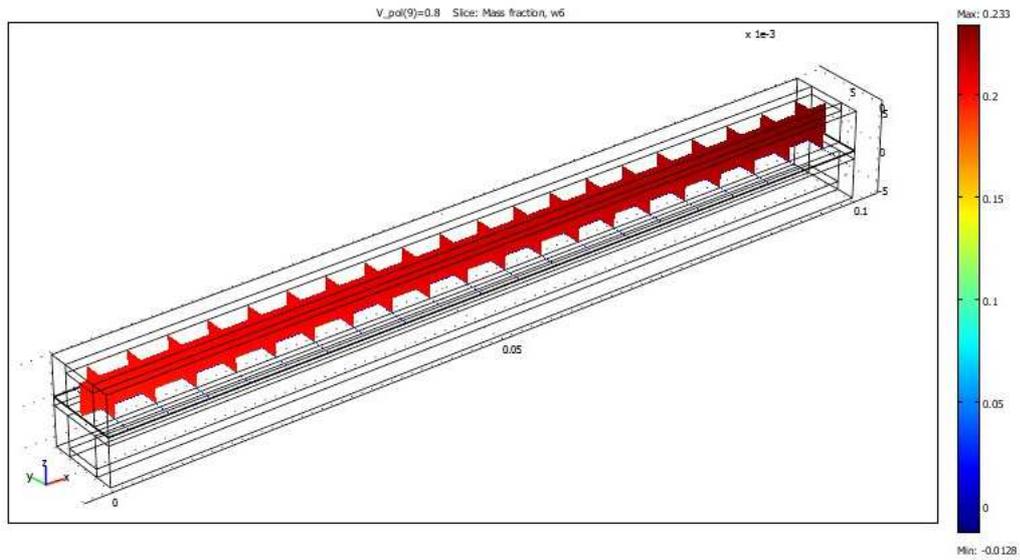
Fig.5. Oxygen distribution in the cathode at 0.5 V cell voltage.

76
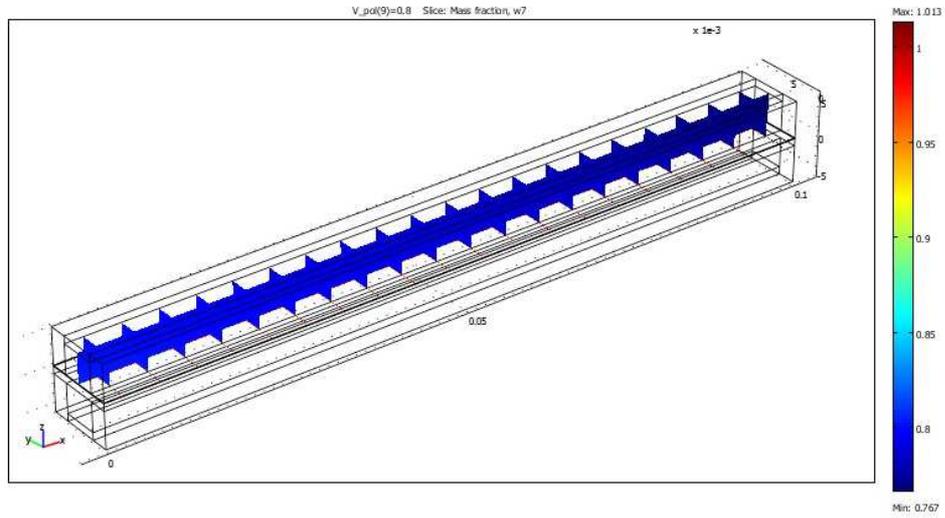
Fig.6. Nitrogen distribution in cathode at 0.5 V cell voltage.
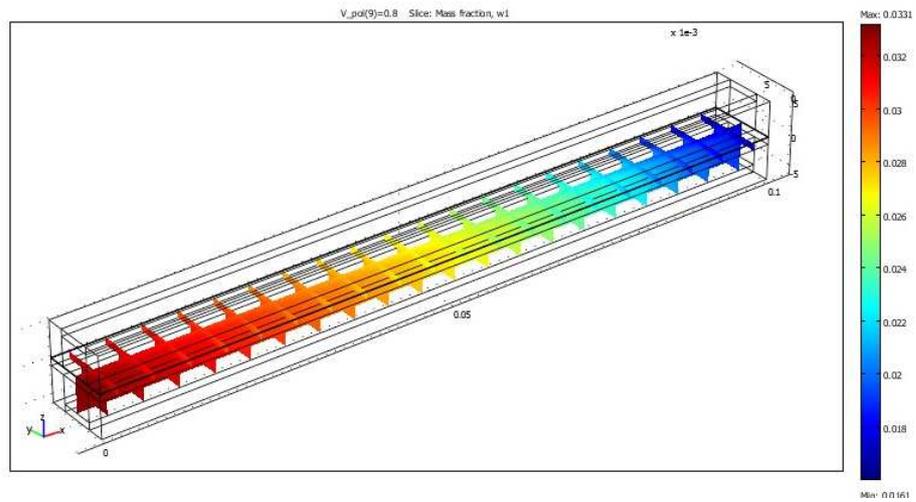
Fig.7. Hydrogen distribution in the anode at 0.5 V cell voltage.
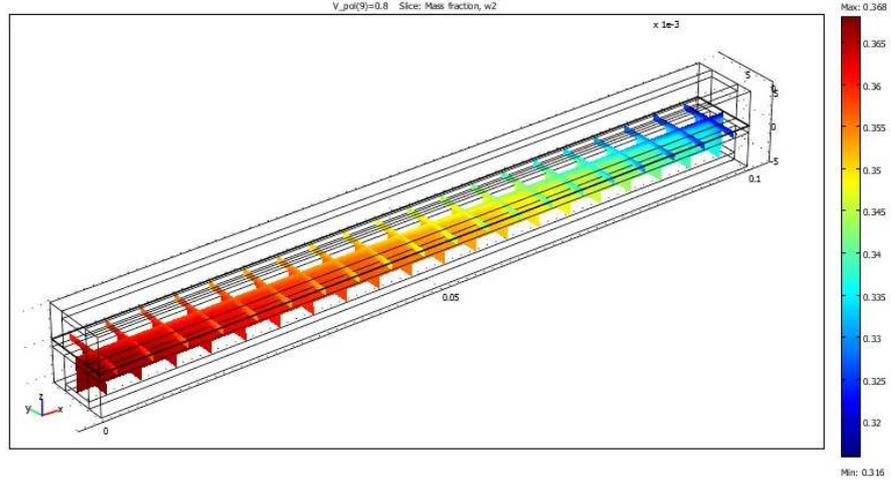
Fig.8. H_2O distribution in the anode at 0.5 V cell voltage.
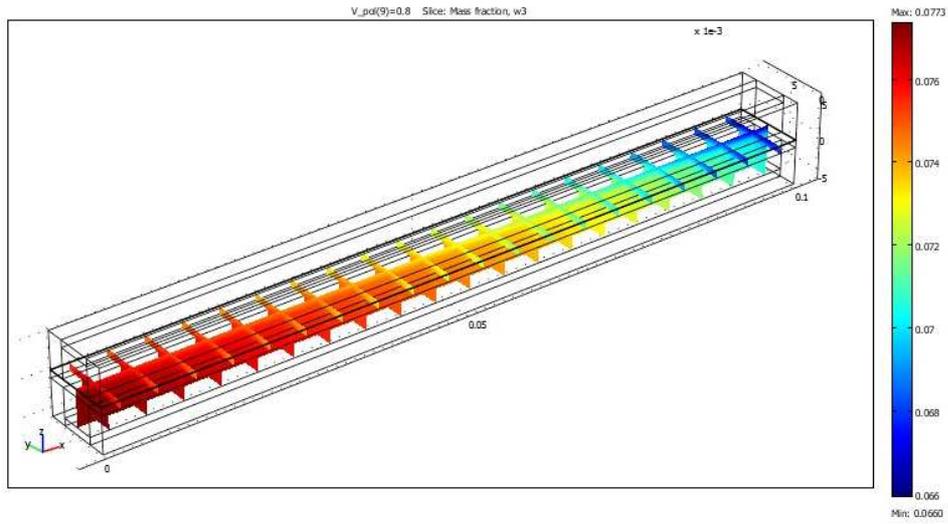
Fig.9. CO distribution in the anode at 0.5 V cell voltage.
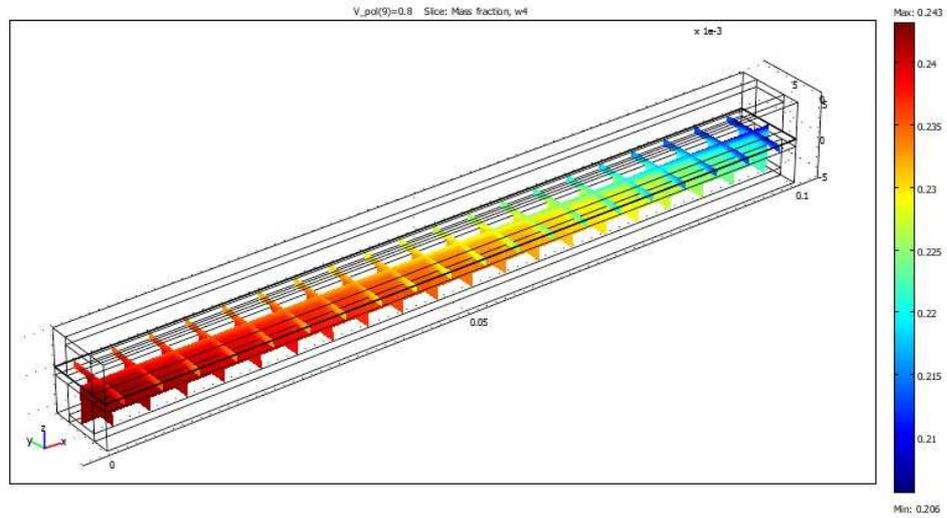
Fig.10. CO_2 distribution in the anode at 0.5 V cell voltage.
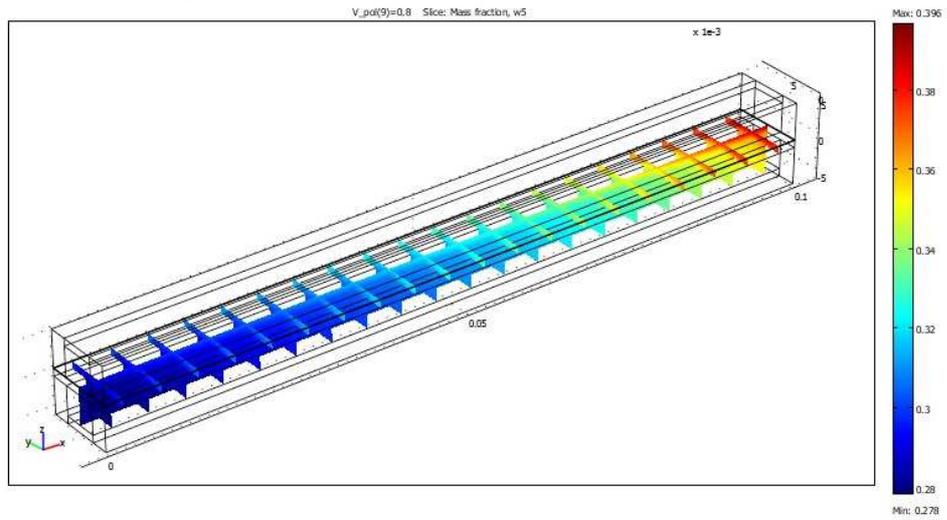
Fig.11. Nitrogen distribution in the anode at 0.5 V cell voltage.
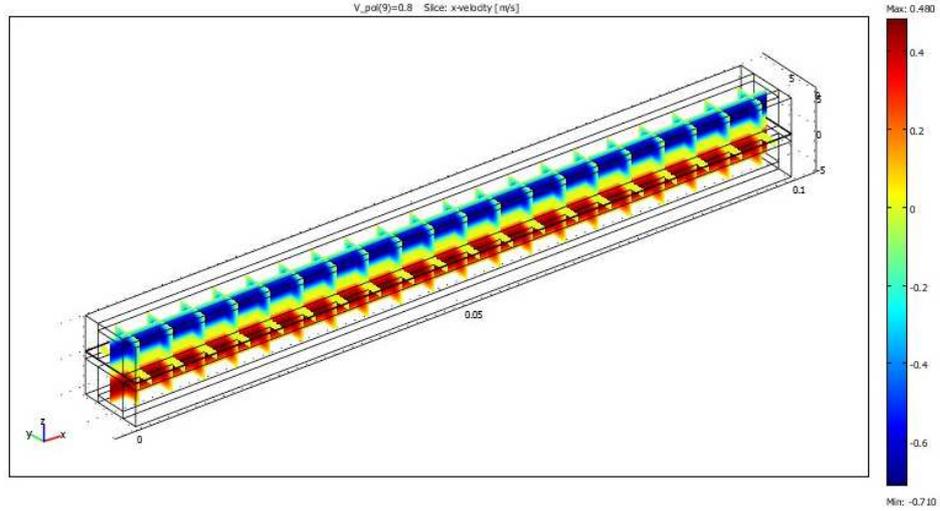
Fig.12. Velocity distribution in the anode at 0.5 V cell voltage.

Figure 13 shows the voltage as a function of the total current (polarization curve). The effect of operating temperature and tortuosity of the porous layers on the performance of an anode-supported SOFC is shown in Fig. 14 and Fig. 15, respectively.
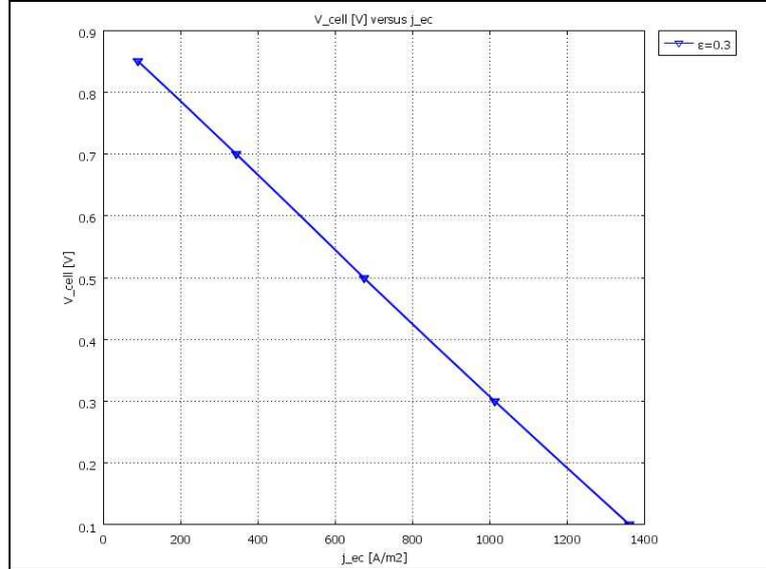
Fig.13. Polarization curve
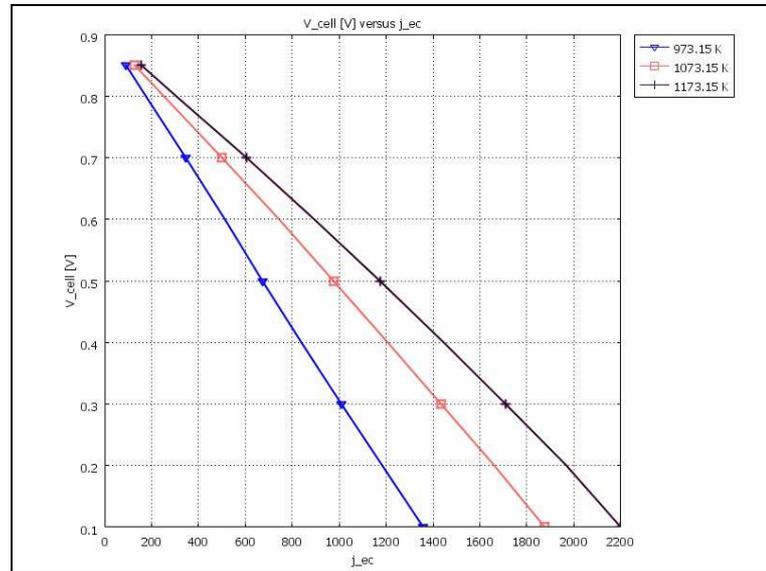
Fig.14. Effect of operating temperature on the performance of an SOFC.

81
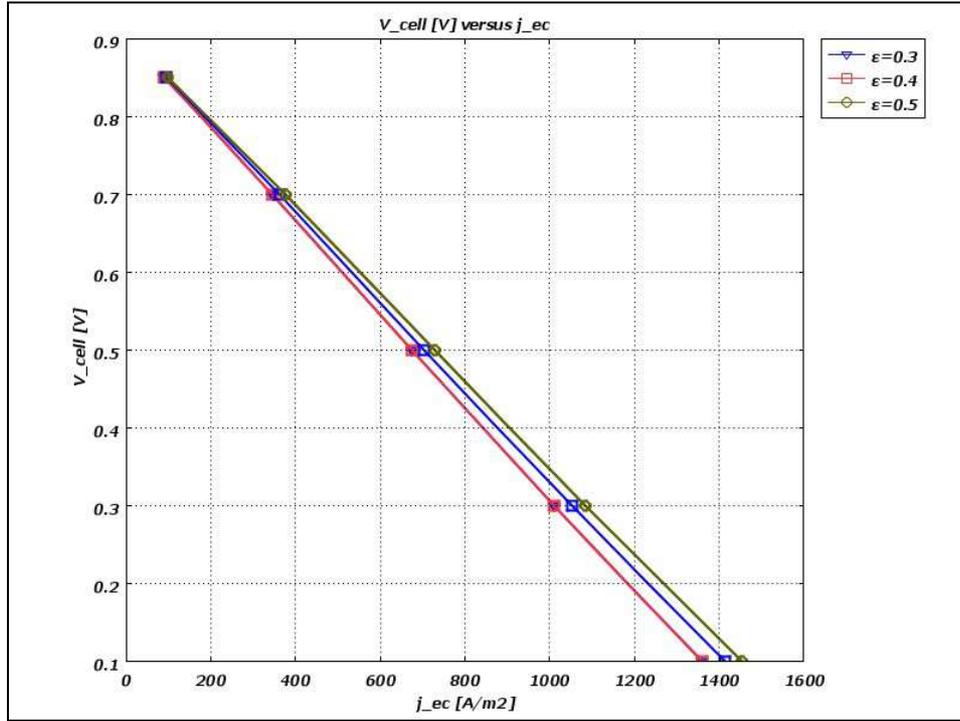
Fig.15. Effect of porosity on the performance of an SOFC.

A consequence of the concentration distribution is that the current density will be nonuniform in the electrodes. Figure 16 depicts the current density distribution at the cathode side of the ionic conductor.
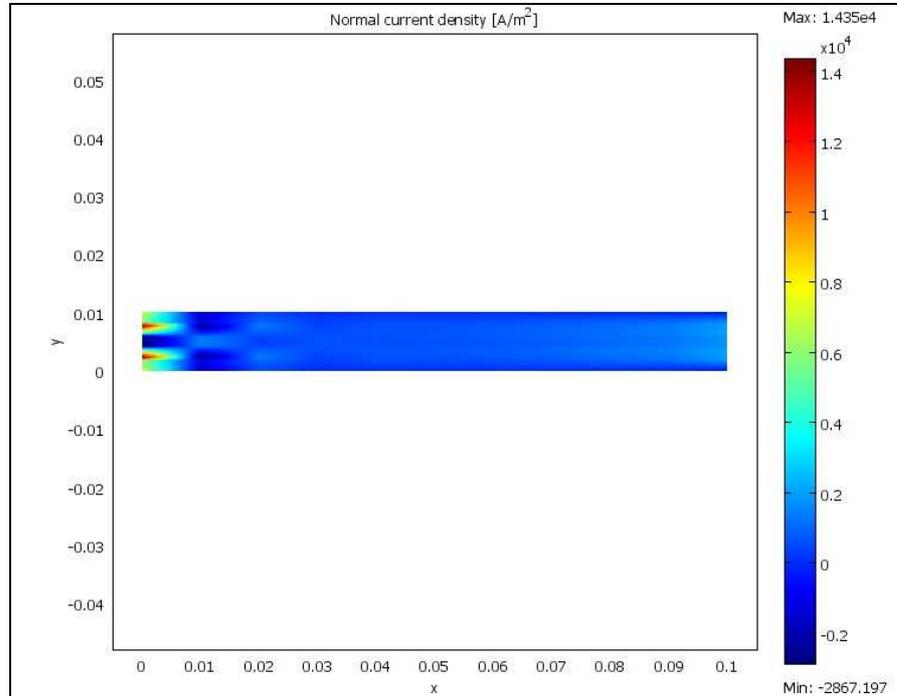
Fig.16. The current density in the unit cell operating at 0.5 V

Figure 17 shows the power output as a function of the current density. The model predicts a maximum power-output of 325 W/m^2 for the at 700 A/m^2 for unit cell.
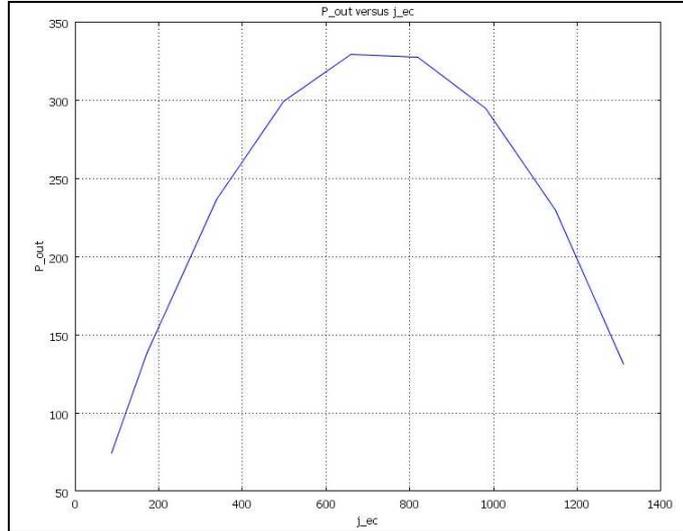
Fig.17. Power output as a function of current density.

Figure 18 shows the power output as a function of the cell voltage. The model predicts a maximum power-output of 325 W/m2 at 0,5 V for the unit cell.
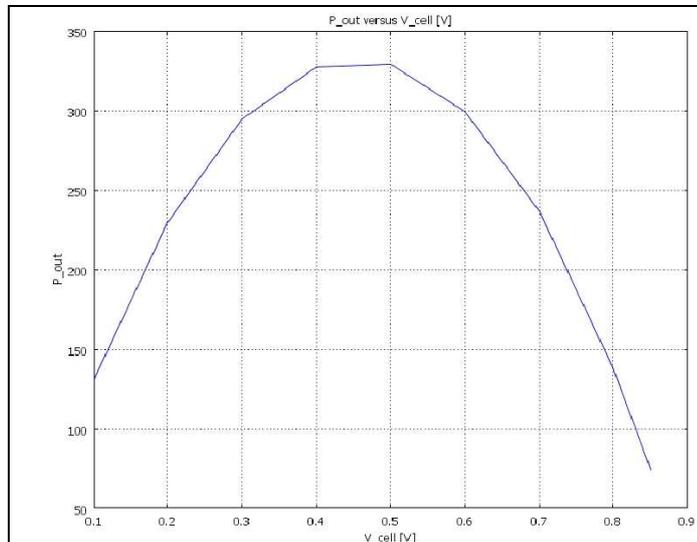
Fig.18. Power output as a function of cell voltage.

6. Conclusions

In this paper, a 3D steady-state model of an anode-supported planar solid oxide fuel cell (SOFC) was presented. The finite element commercial package, COMSOL 3.5, was used to solve a set of governing equations. The mathematical analysis has been developed by using finite element method, experimental data from literature, and solving the governing equations numerically to predict SOFC performances with different operating conditions and with different material properties.

Given a cell geometry, the performance of a SOFC strongly depends on the operating conditions and the inlet fuel composition. Since SOFCs offer a wide range of operating possibilities, identifying the effect of operating conditions such as air flow rate and inlet fuel composition on the efficiency and power density are critical for optimal operation of SOFCs.

As a consequence of oxygen depletion, the current density distribution is poor, with most of the current produced close to the cathode inlet. In addition, the current collector's position is detected, which corresponds to a slightly increased current density on its edges. This means that the cell is not used optimally. One way to improve the operating conditions is to increase the cathode flow rate, thus improving the oxygen mass transport.

It is seen increasing the porosity of the porous layers and temperature increases the performance of an anode-supported SOFC performance.

REFERENCES
[1] U.S. Department of Defense, 2006, MIL-DTL-16884L, Detail Specification Fuel Naval Distilate
[2] R. Suwanwarangkul, E. Croiset, M.W. Fowler, P.L. Douglas, E. Entchev, M.A. Douglas, Performance comparison of Fick's, dusty-gas and Stefan–Maxwell models to predict the concentration overpotential of a SOFC anode, Journal of Power Sources 122 (2003) 9–18
[3] K.J. Daun, S.B. Beale, F. Liu, G.J. Smallwood, Radiation heat transfer in planar SOFC electrolytes, Journal of Power Sources 157 (2006) 302–310
[4] Andreassi L., Toro C., Ubertini S., 2007. Modeling carbon monoxide direct oxidation in solid oxide fuel cells. In Proceedings ASME European Fuel Cell Technology and Applications Conference, EFC2007-39057.

[5]   C.F. Curtiss and R.B. Bird, Ind. Eng. Chem. Res., vol. 38, p. 2515, 1999.

[6]   Perry RH. et al.,1997, Perry's chemical engineers' handbook. seventh ed.,New York: McGraw-Hill

[7]   Matthew M. Mench, Fuel Cell Engines, 2008 by John Wiley & Sons, Inc.

[8]   Dong Hyup Jeon, A comprehensive CFD model of anode-supported solid oxide fuel cells, Electrochimica Acta 54 (2009) 2727–2736

[9]   Ezgi, Cüneyt, Design And Analysis Of NATO F-76 Diesel Fueled Solid Oxide Fuel Cell System Onboard Surface War Shıp Ph.D. Thesis, Ege University,Turkey (2009).

[10] Bossel, U., 1992, "Facts and Figures, Final Report on SOFC Data", Swiss Federal Office of Energy, Operating Task II, Berne, Switzerland, April,

[11] Yakabe H, Sakurai T.,2004, 3D simulation on the current path in planar SOFCs Solid State Ionics, 174:295–302.

[12] Shi Yixiang, Cai Ningsheng, Li Chen., 2007, Numerical modelling of an anode-supported SOFC button cell considering anodic surface diffusion. J Power Sources 164:639–48.

[13] Hocine Ben Moussa, Bariza Zitouni, Kafia Oulmib, Bouziane Mahmahc, Maiouf Belhamelc, Philippe Mandind,2009, Hydrogen consumption and power density in a co-flow planar SOFC, International journal of hydrogen energy.

[14] R.B. Bird, W.E. Stewart, and E.N. Lightfoot, Transport Phenomena, Second edition, John Wiley & Sons, 2005.